SCIENTIFIC REPORTS

OPEN

Bayesian-Driven First-Principles Calculations for Accelerating Exploration of Fast Ion Conductors for Rechargeable Battery Application

Randy Jalem[1,2,3], Kenta Kanamori[4], Ichiro Takeuchi[3,4,5], Masanobu Nakayama[2,3,6,7], Hisatsugu Yamasaki[8] & Toshiya Saito[8]

Safe and robust batteries are urgently requested today for power sources of electric vehicles. Thus, a growing interest has been noted for fabricating those with solid electrolytes. Materials search by density functional theory (DFT) methods offers great promise for finding new solid electrolytes but the evaluation is known to be computationally expensive, particularly on ion migration property. In this work, we proposed a Bayesian-optimization-driven DFT-based approach to efficiently screen for compounds with low ion migration energies (E_b). We demonstrated this on 318 tavorite-type Li- and Na-containing compounds. We found that the scheme only requires ~30% of the total DFT-E_b evaluations on the average to recover the optimal compound ~90% of the time. Its recovery performance for desired compounds in the tavorite search space is ~2× more than random search (i.e., for $E_b < 0.3\,eV$). Our approach offers a promising way for addressing computational bottlenecks in large-scale material screening for fast ionic conductors.

There has been a rapidly growing interest to systematically search for new fast ionic conductors using high-throughput calculations, particularly by leveraging from the wealth of material information from crystal structure databases[1–5]. The workhorse simulation tool that is often employed in these tasks has been based on first-principles density functional theory (DFT)[6,7] which can offer a level of predictive accuracy that is comparable to experimental results[8–10]. However, DFT-based material search with transition state property criterion (e.g., E_b) is still few and of limited scope[11–14]. The relatively high calculation costs involved make these efforts very tedious and in most cases impractical[15–17]. Other cheaper methods have been utilized as substitutes and for rough screening, one of these is by force-field (FF) approach such as bond valence summation[18]. However, the drawback of FF is that its accuracy is strongly tied to the quality of its fitted empirical parameters and the choice of the functional forms used to approximate interatomic bonding potentials. The task of fitting for FF parameters, which relies on experimental and/or DFT data, is also time-consuming. As a result, it is technically challenging to obtain a truly robust FF parameter set that can be applied for a large variety of structures and chemistries.

[1]Japan Science and Technology Agency (JST), PRESTO, 4-1-8 Honcho Kawaguchi, Saitama, 332-0012, Japan. [2]National Institute for Materials Science – Global Research Center for Environment and Energy based on Nanomaterials Science (NIMS-GREEN), 1-1 Namiki, Tsukuba, 305-0044, Ibaraki, Japan. [3]Center for Materials research by Information Integration (CMI²), Research and Services Division of Materials Data and Integrated System (MaDIS), NIMS, 1-2-1 Sengen, Tsukuba, 305-0047, Ibaraki, Japan. [4]Department of Computer Science/Research Institute for Information Science, Nagoya Institute of Technology, Gokiso-cho, Showa-ku, Nagoya, Aichi, 466-8555, Japan. [5]RIKEN Center for Advanced Intelligence Project, 1-4-1 Nihonbashi, Chuo-ku, Tokyo, 103-0027, Japan. [6]Frontier Research Institute for Materials Science (FRIMS) & Department of Advanced Ceramics, Nagoya Institute of Technology, Gokiso-cho, Showa-ku, Nagoya, 466-8555, Aichi, Japan. [7]Elements Strategy Initiative for Catalysts and Batteries, Kyoto University, f1-30 Goryo-Ohara, Nishikyo-ku, 615-8245, Kyoto, Japan. [8]Battery Material Engineering & Research Div., Toyota Motor Corporation, 1200, Mishuku, Susono, 410-1193, Shizuoka, Japan. Correspondence and requests for materials should be addressed to R.J. (email: JALEM.Randy@nims.go.jp)

The difficulty of keeping the computational cost manageable in DFT-based material search/screening has also made it prohibitive to readily expand the search space by ionic substitution, for example, in known database compounds. Nonetheless, there is a huge merit for checking these gaps in the composition space because they could be fertile grounds for new materials[19]. In fact, a number of discoveries up to date were realized even with only a select few number of substitutions, such as in the case of Li/Na ionic conductors: layered-type AMO_2 (A: Li, M:Co, Ni,)[20,21], olivine-type $AMPO_4$ (A: Li; M: Fe, Mn)[22], garnet-type $Li_7La_3Zr_2O_{12}$[23], and tetragonal $A_{10}MP_2S_{12}$ (A: Li, Na; M: Ge, Sn)[24,25].

In order to take advantage of the accuracy of DFT for predicting transition state properties and to extend today's material search for fast ionic conductors beyond the known database composition space, two major computational cost issues need to be tackled: (i) the inherent cost for calculating transition state properties itself (such as for E_b) and (ii) the cost due to the combinatorial complexity arising from ionic substitution in known structure types. Meanwhile, traditional regression/classification techniques are limited with issues in terms of material discovery: (i) fitting precision and uncertainty issue which is linked to the need for larger and larger training dataset as the search space also becomes larger (i.e., to improve out-of-sample prediction) and (ii) the cost of building sufficient training data especially for calculation-intensive target properties (eg., E_b, ionic conductivity in rechargeable Li ion batteries). Our proposed solution, as will be further explained later, is to formulate an appropriate search/screening strategy in which instead of exhaustive or random searches, calculation resources are selectively allocated on compounds that would likely demonstrate fast ionic conduction, or in the case here, compounds with low E_b values. On the other hand, calculations for compounds with high E_b values are to be minimized, if not totally avoided. This strategy can be formalized as the process of solving an optimization problem, but its objective function (i.e., for E_b) cannot be directly expressed analytically. Conventional optimization approaches such as convex optimization and gradient descent are not straightforward to implement in such cases.

Recently, machine learning algorithms based on Bayesian optimization (BO) have become increasingly popular for efficiently solving material science problems. Unique from traditional machine learning methods (eg., LASSO and neural network), BO constructs a probabilistic model for the objective function and then exploits this model for deciding the next query point to be evaluated. BO has been successfully used in crystalline interface optimization[26], construction of interatomic potentials[27], and low-energy region identification in a potential energy surface[28]. Studies have also shown to implement BO together with DFT in order to find single- and binary-component solids with high melting temperature[29], compounds with low lattice thermal conductivity[30], and ternary compounds with desired elastic properties[31]. These demonstrations are indeed a step towards a sound and efficient design of new materials.

Our present work is also aimed towards finding new materials in an enhanced iterative-driven manner, but this time the chemical search space is a quinary system with battery as the target application and with the use of a transition state property as a practical search criterion – E_b. Quinary system is a challenging but highly relevant search space for battery research because many relevant materials and their optimization lies in this composition space. Examples include $Li_{7-x}La_3Zr_{2-x}Ta_xO_{12}$ solid electrolytes which has an optimized ionic conductivity on the order of 10^{-3} S/cm[32], $LiNi_xMn_yCo_zO_2$ cathodes which show good specific energy and specific power density[33], and $Na_3Ti_2P_2O_{10}F$ which is a new candidate anode material for sodium ion batteries[16,34,35]. Moreover, the E_b criterion, which can also be experimentally accessed (eg., by impedance measurements and NMR), is a very important metric for battery researchers since it is ubiquitous in all of the critical device components (anode, cathode, and electrolyte). Previous efforts have dealt mainly on unary and binary systems, whereas the present study emphasized on formulating an efficient and automation-compatible property-based search/screening in the extended composition space of five-component compounds with a fixed crystal structure (tavorite $AMXO_4Z$ system, where A, M, X, and Z are sites for ionic substitution), covering yet-to-be synthesized chemistries that are not yet found in databases. The choice of tavorite $AMXO_4Z$ is motivated by the idea that it is relatively unexplored in terms of varying its composition, so there is a good possibility of finding truly unreported new compounds[36–38]. Another reason is that one of the reported compound, $LiFeSO_4F$, demonstrates high Li insertion rate which means that pathways within the structure can be highly favorable for ion transport[36]. Ion migration property in crystalline solids (i.e., E_b), to the best of our knowledge, still has no published databases up to now (experimental or computational) and also, by DFT, incurs significantly higher calculation costs than, for example, thermodynamic property-based search criteria (as in some of the previous works mentioned above[26,28,29,31]). We also demonstrate concretely in this work the ability of BO for knowledge transfer in a successive screening scenario, that is, using the posterior from one screening task as a prior for the next screening task. Finally, we also aimed to devise a practical workflow for automated material search/screening that is flexible enough to handle a large number and variety of material descriptors, this is realized by coupling the workflow with a modified BO scheme that is general for high dimensions[39–42]. We then use the BO probabilistic model to find compositions of low E_b for Li and Na ions within the database-reported ordered tavorite structure. The target application for the tavorite-type ionic conductors is for solid electrolyte use, so only compounds that do not permit electronic conduction are considered (i.e., no transition metals are included for ionic substitution).

Results

Chemical search space and crystal structure description. Tavorite-type compounds with a general formula $AMXO_4Z$ (A: Li, Na; M: group 2, 3, 4, 13 elements; X: group 14, 15, 16 elements; Z: F, Cl, Br, I) were targeted for the E_b-based solid electrolyte screening. The model crystal structure ($P\bar{1}$) is shown in Fig. 1a with the host framework comprising with MO_4Z_2 octahedra (M 1a, 1h; O 2i) and XO_4 tetrahedra (X 2i; O 2i). The MO_4Z_2 octahedra are corner-linked together at their *trans*-Z atoms to form chains along [111]. Each oxygen atoms from these chains are in turn shared with X atoms which then assumes a tetrahedral environment. Site splitting occurs for the A atoms (2i). Overall, the search space includes $LiMXO_4F$ dataset taken from our previous work[13] and
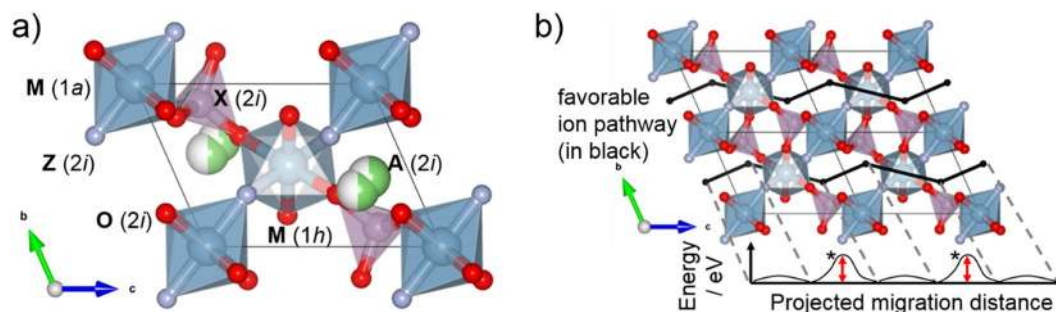
Figure 1. (**a**) Model unit cell for the tavorite $AMXO_4Z$ ($P\bar{1}$) showing various crystallographic sites and polyhedral units. Green/white spheres for A atoms indicate a splitting site. (**b**) The predicted favorable conduction pass for A cations within the tavorite framework (A atoms removed) as shown in its $1 \times 2 \times 2$ supercell (in black, along c-direction) (13). The local barrier height E_b marked by asterisks are equivalent characteristic path bottlenecks. The VESTA software was uses for structure visualization[43].
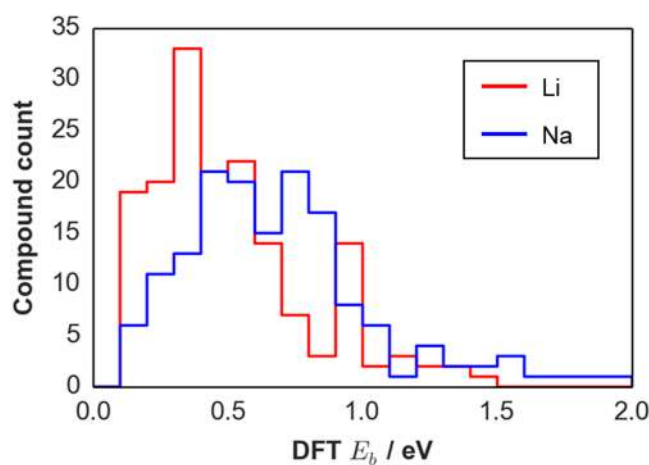

Figure 2. Sample distributions for the $DFT\text{-}E_b$ datasets prepared for the BO-driven search of tavorite $AMXO_4Z$ solid electrolytes. There are 163 and 154 DFT-E_b samples contained in the Li and Na dataset, respectively (see Supplementary Table S2 for the actual values).

newly calculated datasets for $LiMXO_4(Cl/Br/I)$ and $NaMXO_4(F/Cl/Br/I)$. Although there are different local A cation pathways in the tavorite structure, our previous calculations determined that its ionic conduction is anisotropic, with the dominant transport pathway being facile in one major cell direction[13]. This conduction pass is defined by a series of local site-to-site jump environments, each sandwiched between two MO_4Z_2 octahedra. Hence, E_b sampling by NEB method was carried out only at the characteristic local pathway bottleneck, as shown in Fig. 1b in asterisk.

DFT-E_b dataset. Figure 2 shows the distribution of Li and Na DFT-E_b datasets (a total of 318 samples) that were prepared in advance for the BO-driven search. We note that although the dataset size may not be large enough for practical material discovery, it should be sufficient enough (considering the heavy computation cost of DFT approach for kinetics-related properties) for evaluating how fast BO-driven search can find the best or nearly-best one in a quinary system. Differences in the sample distribution of the two datasets are revealed by estimating their sample statistics such as maximum E_b ($E_{b,max}$), median E_b ($\widetilde{E}_b$), and skewness ($\hat{\alpha}_3$) and kurtosis ($\hat{\alpha}_4$): quantities are $\{E_{b,max} = 1.424\,eV, \widetilde{E}_b = 0.448\,eV, \hat{\alpha}_3 = 0.960, \hat{\alpha}_4 = 0.488\}$ and $\{E_{b,max} = 1.965\,eV, \widetilde{E}_b = 0.661\,eV, \hat{\alpha}_3 = 1.111, \hat{\alpha}_4 = 1.594\}$ for Li and Na, respectively. This comparison clearly shows that the Na case has a broader range and more samples with large E_b which could mainly stem from the larger atomic mass and ionic radius of Na ($r_{Na^+} = 1.02\,Å$ vs. $r_{Li^+} = 0.76\,Å$ for an octahedral environment)[44]. On another note, both distributions are positively skewed ($\hat{\alpha}_3 > 0$) but with the Na case having a heavier tail towards large E_b values ($\hat{\alpha}_{4,Na} > \hat{\alpha}_{4,Li}$). These datasets should provide a more stringent performance check for the BO-driven search since random search can favorably sample in the low-E_b density region. The optimal compounds ($\boldsymbol{x}_*$) in the Li and Na datasets are $LiScSbO_4I$ ($E_b = 0.104\,eV$) and $NaErAsO_4Cl$ ($E_b = 0.116\,eV$), respectively; both are still unreported compounds.

BO-driven DFT-E_b search workflow. Figure 3 shows the schematic workflow for the E_b-based BO-driven search within the $AMXO_4Z$ tavorite search space. At first, the search space of compounds is populated by various ionic substitutions at the A, M, X, and Z sites. Next, $t = 5$ initial randomly picked compounds ($\{\boldsymbol{x}_i\}_{i=1}^{t=5}$) are sampled
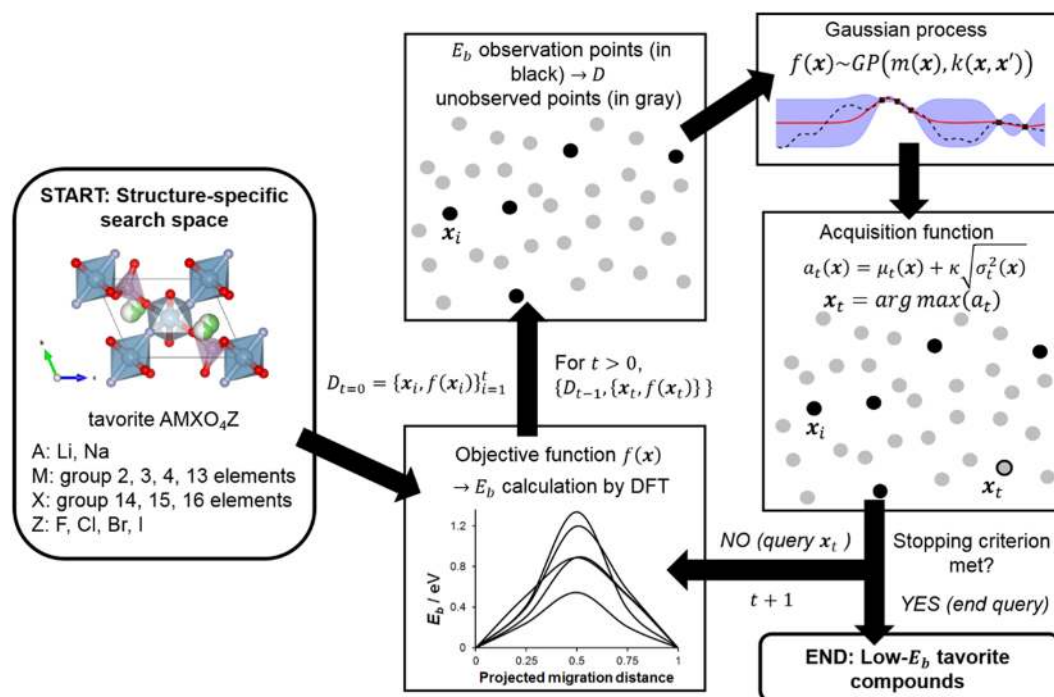
Figure 3. Schematic workflow for the proposed BO-driven DFT-E_b search for tavorite $AMXO_4Z$ compounds.
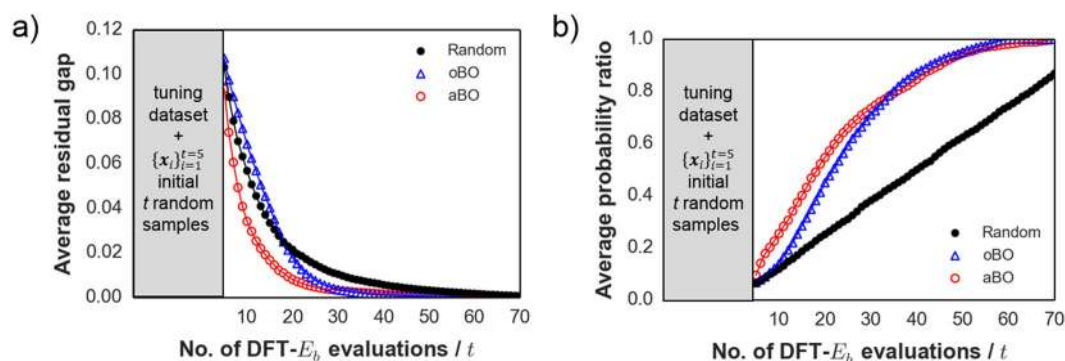
Figure 4. (**a,b**) Performance comparison for additive BO (aBO), ordinary (oBO), and random search using the Li-tavorite dataset (averaged from 1000 trials). Horizontal axes for both denote the sequential number of DFT-E_b evaluations t. The vertical axis in a) shows the residual gap at step t between optimal $f(x_*)$ and the prior best solution ($max_{x_{1:t}} f(x_t)$). The vertical axis in (**b**) shows the average probability ratio of discovering the optimal Li-tavorite compound x_*. Note that both additive BO (aBO) and ordinary BO (oBO) search methods here used the tuned hyperparameters from half of the Li dataset excluded for search performance comparison (gray area).

for DFT-E_b for training the Gaussian Process GP model. The model posterior then provides the predictive mean function $\mu_t(x)$ and a predictive variance function $\sigma_t^2(x)$ which then defines the acquisition function $a(x)$. Maximizing $a(x)$ then enables for deciding the next query compound x_t to be evaluated for DFT-E_b. The sequence is continued until a user-defined number of evaluations or stopping criterion is achieved. In this work, the number of function evaluations was set equal to the number of test data samples.

Performance evaluation of BO approach.　In this paper, the additive BO model is labeled as aBO while the ordinary BO model is labeled as oBO. Figure 4a shows the efficiency of the three search methods for minimizing the residual gap at each evaluation step t between optimal $f(x_*)$ and the current best solution ($max_{x_{1:t}} f(x_t)$) for the Li test data. In the high uncertainty regime ($t < 20$) of the simulated search (i.e., high σ^2 since majority of test data compounds are still unobserved), aBO shows the best performance. Meanwhile, oBO performs slightly poorer than random search but when $t > 20$, it starts to outperform. This behavior for oBO especially at the early stage of the search can be explained by its kernel complexity and the skewed E_b distribution (see Fig. 3). It should be emphasized though that the nature of the distribution for $f(x)$ is usually not known in advance but incidentally
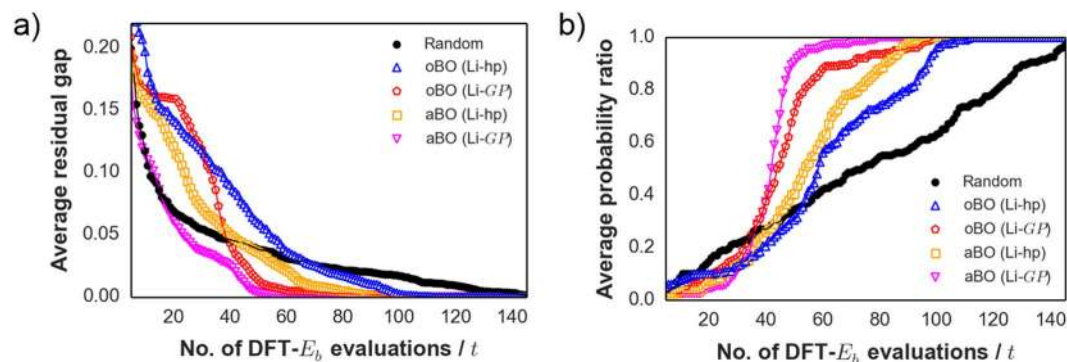
Figure 5. (**a**,**b**) Performance comparison for additive BO (aBO), ordinary BO (oBO), and random search using Na dataset (averaged from 50 trials). Two transfer settings for BO were used: transferred hyperparameters only (Li-hp) and with both transferred hyperparameters and posterior GP (Li- GP) from Li dataset for BO. Horizontal axes for both denote the number of $f(\boldsymbol{x})$ evaluations for DFT-E_b. The vertical axis in a) denotes the residual gap at each evaluation step t between optimal $f(\boldsymbol{x}_*)$ and the prior best solution ($max_{\boldsymbol{x}_{1:t}} f(\boldsymbol{x}_t)$). The vertical axis in (**b**) denotes the percentage ratio of discovering the optimal Na-tavorite compound $\boldsymbol{x}_*$.

even with a non-normal distribution the BO approach is still generally efficient in querying for low-E_b compounds. Figure 4b shows an alternative performance comparison analysis which is based on the probability ratio of discovering the optimal Li-tavorite compound $\boldsymbol{x}_*$ as the number of observations t increases (again, as averaged over 1000 trials). The plot indicates that at $t = 35$, there is already ~80% probability of discovering $\boldsymbol{x}_*$ for both BO-driven searches.

Figure 5a shows the search performance of the 3 methods, for the Na dataset: random search, oBO search, aBO search. Two transfer settings for BO were used: transferred hyperparameters only (Li-hp) and with both transferred hyperparameters and posterior GP (Li- GP) from Li dataset for BO. The plots are averaged over 50 trials for a search space of 154-compounds test data. For $t < 40$, oBO is overall performing poorer than random search and aBO regardless of the inherited model settings. This can be primarily explained in a similar fashion as with the Li case, that is, from the viewpoint of kernel complexity and high estimation error when the number of unobserved compounds is still high. Out of the 5 tested models, Li-GP aBO gains a clear advantage over random search for $t > 20$. These results validate the use of model transfer and demonstrate the predictive power of the trained GP model from the Li dataset for the Na dataset. Additionally shown in Fig. 5b is the probability ratio of finding the optimal Na-tavorite compound $\boldsymbol{x}_*$. At $t = 50$ evaluation steps (i.e., ~30% of the search space observed), Li-GP aBO and Li-GP oBO can find $\boldsymbol{x}_*$ ~90% and ~80% of the time, respectively.

Na and Li ionic conductivity (or Li and Na ion migration energy) are inherently different properties and normally cannot be optimized simultaneously. However, with the systematic approach of knowledge transfer such as in the problem setting (i.e., from Li to Na system), we demonstrated that indeed we can efficiently optimize and find the optimal compound(s) better than random method.

The goal of the BO-driven search can be modified so that compounds that satisfy a cutoff value are explicitly searched, in contrast with just finding the single most optimal compound $\boldsymbol{x}_*$. To demonstrate this, we used the Li-GP transfer model setting and set a criterion of $E_b < 0.3$ eV, referred from perovskite $Li_{0.34}La_{0.51}TiO_{2.94}$ solid electrolyte[45]. The Na dataset was used for performance check and results are displayed in Fig. 6. The vertical axis represents the average number of desired compounds found, which for the Na dataset, would be 17 total compounds meeting the cutoff. For $t < 50$ (~30% search space coverage), aBO found twice the number of desired compounds than oBO and Random search, discovering ~73% (12.40 compounds) as compared to ~37% (6.26 compounds) and ~33% (5.54 compounds), respectively. However, we note here that aBO failed to find the remaining compounds with $E_b < 0.3$ eV even up to ~80% search space coverage ($t = 130$). This issue is due to the method trading off some of its predictive accuracy for model flexibility. Still, aBO demonstrates its remarkable performance and suitability for large-scale material screening tasks, given that the search is prioritized on maximizing search hits for desired compounds with as few number of DFT-E_b calls as possible.

Descriptor contribution towards E_b prediction. Another advantage of additive Bayesian optimization is that the importance of each group of descriptors can be easily interpreted. Figure 7 shows the contributions of descriptor groupings for Li-GP aBO towards E_b prediction. The degree of contribution was calculated by taking the normalized ratio of the covariance amplitude σ_f^2 for each groups. The two main contributions came from descriptor groups related to the RDF features (g5) and lattice cell features (g1). Meanwhile, inter-polyhedron features (g4) does not contribute and thus could be removed, reducing model complexity from $M = 5$ down to $M = 4$ terms. This non-contribution of inter-polyhedron features may be explained by their redundancy since the interatomic-based information contained in them could have been well-expressed already or have been better expressed by RDF features (g5). RDF features, on the other hand, are determined here as effective descriptors for the prediction of E_b with an inherently structure-independent nature, making it directly applicable for material search/screening tasks with multiple structure types.
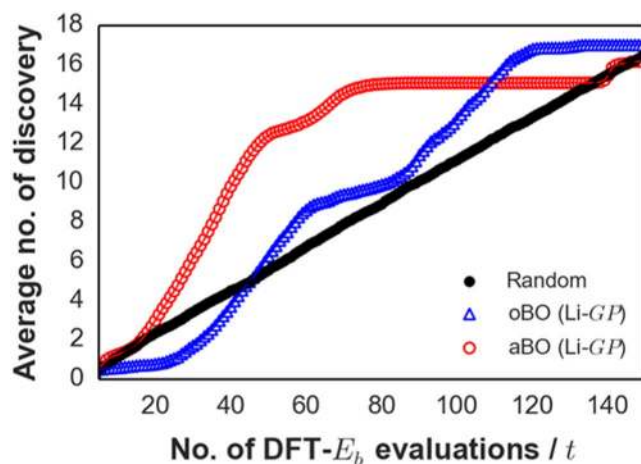
Figure 6. Average number of discovered Na-tavorite compounds with $E_b < 0.3$ eV vs. number of DFT evaluations.
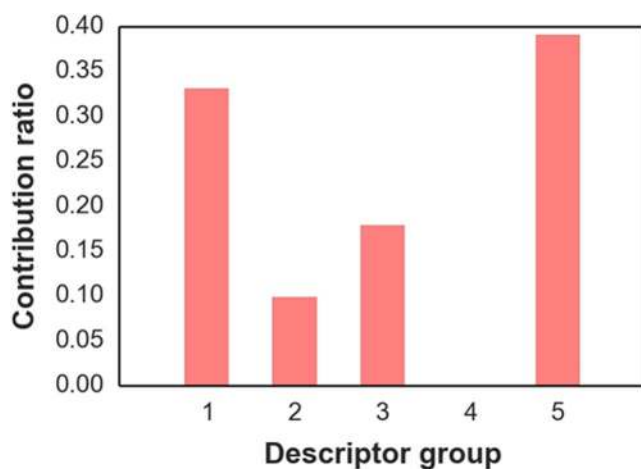

Figure 7. Descriptor group contributions toward E_b prediction as based from Li-GP aBO model. Vertical axis shows the ratio related to the covariance scale σ_f^2 of each descriptor group as determined by marginal likelihood maximization.

To investigate the characteristics of the descriptor values among different compounds, we analyzed the data distribution of some descriptors. We used g1 descriptors (lattice cell features) which were determined automatically by the present BO method as significantly contributing towards E_b prediction (see Supplementary Fig. 4). We observed that for g1 descriptors, there are different distribution shapes, modalities (unimodal, multi-modal) and degree of skewness for the distribution of values which are indicative of variability and variety in the captured information. In addition, the ranges of each descriptor distributions (see Supplementary Table 5) indicate a varying degree of closeness of values among compounds. Nevertheless, g1 descriptors may be generally regarded as sufficiently differentiating for tavorite compounds. As an example, we examined descriptor df which represents the path bottleneck size for the migrating ion. A value of 0.707 Å (minimum among compounds) would make it geometrically unfavorable for Li ion to pass through (Li ionic radius is 0.76 Å in octahedral coordination, as in the tavorite structure), and much more unfavorable for Na ion (1.02 Å)[44]. Meanwhile, a value of 2.240 Å (maximum among compounds) means both Li and Na ion can pass through geometrically.

Based from above importance analysis on descriptor group contributions, we have shown that our chosen set of descriptors and the strategy of grouping them in their natural groups to define sub-kernel spaces for the BO method is indeed an effective approach for navigating the ion migration energy landscape of the tavorite $AMXO_4Z$ search space.

Post-processing of E_b-screened tavorite compounds. In an actual material screening task, compounds of interest are usually not only evaluated against a single property but also against other metrics. For example, screened compounds after simulated BO can be further narrowed down by thermodynamic stability criterion to assess whether they can be synthesized by experiment or not. For this purpose, we carried out DFT
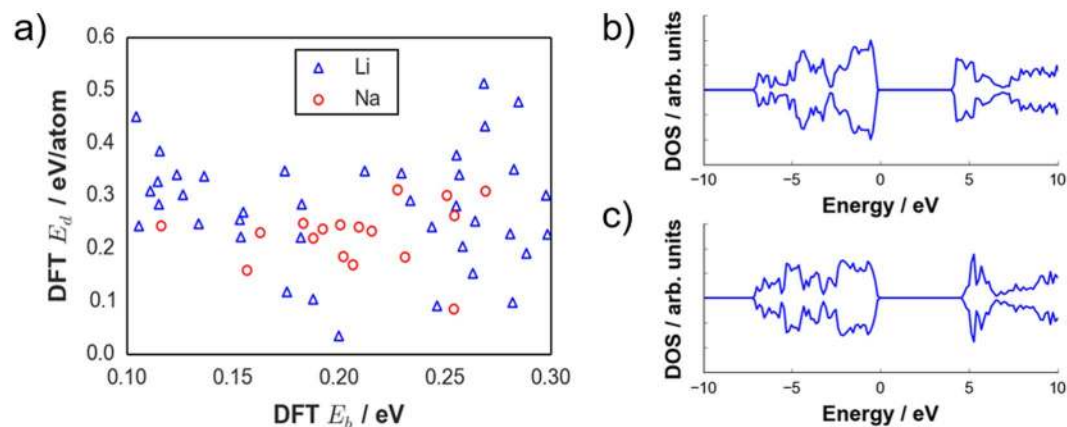
Figure 8. (**a**) DFT-calculated thermodynamic stability energy (E_d) of tavorite compounds with $E_b < 0.3$ eV. Total density of state of screened representative compounds that passed both E_b and E_d cutoffs: (**b**) LiZrGeO$_4$F and (**c**) NaHfSiO$_4$F.

phase stability calculations based on the convex hull approach and aided by the pymatgen library[46,47]. Briefly, the thermodynamic stability energy (E_d) of a given compound was checked against all possible linear combinations of competing phases found in the Materials Project (MP) database[9]. A compound phase may then fall under three cases: (i) $E_d = 0$, the compound is predicted to be at the thermodynamic ground state, (ii) $E_d > 0$, there is a driving force for decomposition, and (iii) for $E_d \approx 0$, a compound is metastable and may be stabilized by appropriate synthesis condition or high kinetic barriers[5]. Based from this classification and from previous empirical results for DFT formation energies, a value of 0.1 eV/atom was chosen as a reasonable upper limit for stability and metastability[5,8].

For the Li-tavorite search space, 20 compounds met the E_d cutoff. Two of these are recorded in ICSD, LiMgSO$_4$F ($E_d = 0.034$ eV/atom) and LiAlPO$_4$F ($E_d = 0.016$ eV/atom), while the rest are hypothetical compounds that are predicted to be experimentally synthesizable. If both E_d and E_b criteria are used, three compounds remained, namely: LiMgSO$_4$F ($E_b = 0.200$ eV, $E_d = 0.035$ eV/atom), LiMgSeO$_4$Cl ($E_b = 0.282$ eV, $E_d = 0.098$ eV/atom), and LiZrGeO$_4$F ($E_b = 0.246$ eV, $E_d = 0.091$ eV/atom). Only LiMgSO$_4$F has been characterized so far as a solid electrolyte, whereas the remaining two are new materials. The other database-reported compound is LiAlPO$_4$F but it did not pass the E_b criterion ($E_b = 0.550$ eV). For the Na-tavorite space, 16 compounds satisfied the $E_d < 0.1$ eV/atom condition, all of them are still unreported. Meanwhile, the hypothetical compound NaHfSiO$_4$F met both E_d and E_b cutoffs ($E_b = 0.254$ eV, $E_d = 0.085$ eV/atom). The E_d values for the next-tier compounds (in the range 0.3 eV $< E_b < 0.4$ eV) are provided in Table S4. Figure 8b,c show the total density of states of LiZrGeO$_4$F and NaHfSiO$_4$F, with DFT-PBE electronic band gap energies determined to be 4.177 and 4.876 eV, respectively. These values are comparable with other known candidate solid electrolytes such as garnet Li$_7$La$_3$Zr$_2$O$_{12}$ (5.79 eV by HSE06) and Li$_{10}$GeP$_2$S$_{12}$ (3.6 eV by PBE) which have wide band gap, indicative of being able to meet the requirement for very low electronic conductivity[48,49]. Additional data are provided in Table S3 for DFT-optimized structural information. The ionothermal synthesis approach would be one of the possible routes for preparing the two new compounds, as demonstrated for already known ones such as tavorite LiMgSO$_4$F[37], and structure-isotopic compounds such as LiFeSO$_4$F[36], LiFePO$_4$F[50], and LiTiPO$_4$F[38,50].

From above results, we have shown that the present DFT-coupled Bayesian optimization approach with additive structure can be applied for quinary systems and when an initial crystal structure type is provided. However, the need for an input structure means that novel compounds with new crystal structures are unsearchable. Nevertheless, we would like to point out that there is now a rich plethora of structure prototypes that can be accessed from existing databases (for example, ICSD presently contains 9,093 structure prototypes)[51]. On another note, other state-of-the-art material search methods have been reported as well, such as crystal structure prediction (CSP) techniques based on evolutionary algorithm[52]. CSP approaches do not require an input structure (the initial atomic arrangement is usually set randomly) but they need composition and initial cell volume. These techniques are meta-heuristic and utilizes empirical rules to govern the search for ground state materials. CSP techniques need to deal with the curse of dimensionality which means that local or global minima structures becomes harder and harder to find as the number of atoms and/or element type increases[52]. Combining our approach with CSP techniques, for example for quinary systems, would be one interesting direction to pursue related to high-dimensionality material search.

Conclusion

A Bayesian-driven DFT-based screening for Li and Na ionic conductors with the tavorite structure was demonstrated using ion migration energy (E_b) as the search criterion. The BO search method was found to be generally more efficient than random search even under a stringent condition of having a positively skewed E_b sample distributions. Using the Na dataset, additive BO with a knowledge transfer setting requires only an average of ~30% search space coverage to recover the optimal compound ~90% of the time. Using the same test dataset and

with a search criterion of $E_b < 0.3\,eV$, additive BO also only needs to observe ~30% of the search space on the average to find ~70% of the total desired compounds, this is twice the recovery performance for desired materials of ordinary BO and random search which can only find ~37% and ~33%, respectively. These performances are realized with the use of effective descriptors, particularly RDF features. Overall, additive modeling can be an effective approach for addressing the high-dimensionality issue in BO-based searches.

Methods

Chemical search space and crystal structure description.
Tavorite-type compounds with a general formula $AMXO_4Z$ (A: Li, Na; M: group 2, 3, 4, 13 elements; X: group 14, 15, 16 elements; Z: F, Cl, Br, I) were targeted for the E_b-based solid electrolyte screening. We note that the M-X cation pair for group 5 and group 13 elements was not included in this study. Although quinary systems have been reported with group 5 cations (e.g., with Ta^{5+} and Nb^{5+} in another structure type[32,53]), group 5 and 13 pairing is highly unlikely in the tavorite structure. This unlikelihood is explained by the deviation of charge distribution for the group 5 - group 13 cation pairing case which leads to a significant destabilization of the crystal structure. The model crystal structure ($P\bar{1}$) is shown in Fig. 1a with the host framework comprising with MO_4Z_2 octahedra (M 1a, 1h; O 2i) and XO_4 tetrahedra (X 2i; O 2i). The MO_4Z_2 octahedra are corner-linked together at their $trans$-Z atoms to form chains along [111]. Each oxygen atoms from these chains are in turn shared with X atoms which then assumes a tetrahedral environment. Site splitting occurs for the A atoms (2i). Overall, the search space includes $LiMXO_4F$ dataset taken from our previous work (13) and newly calculated datasets for $LiMXO_4(Cl/Br/I)$ and $NaMXO_4(F/Cl/Br/I)$.

DFT calculation settings.
The VASP code[54] was used for DFT modeling which applies the projected augmented wave (PAW) approach[55]. The energy for exchange correlation was described in the generalized gradient approximation (GGA) with Perdew-Burke-Ernzernhof formulation for solids (PBEsol)[56]. The initial coordinate dataset for the tavorite structure was referred from available crystal information file (cif) in the Inorganic Crystal Structure Database (ICSD)[52]. With a unit cell of 16 atoms and a spin-polarized condition, a 500-eV cutoff for kinetic energy and a Monkhorst-Pack kpoint resolution of $5 \times 4 \times 3$ were confirmed to show a total energy convergence of less than 1 meV/formula unit (fu). Database-unreported tavorite compounds were calculated using the available experimental cif data as template. The calculation for static atomic charges was based from Bader method[57]. For the dynamical charges, Born effective charge calculation was carried out[58].

The nudged elastic band (NEB) technique was employed to calculate E_b [59]. The unit cell was expanded into a $1 \times 2 \times 2$ supercell and over-the-Brillouin-zone numerical integration was performed by Γ-point sampling. With these conditions, we point out that most of the compounds especially those in the low E_b region were converged to less than 10 meV/fu (with a few compounds with $E_b > 1.5\,eV$ converged to less than 30 meV/fu). After structure optimization on the initial and final state supercell models containing a single A vacancy, seven images in between for the migrating A cation were constructed by linear interpolation. The value of E_b was then calculated according to the formula:

$$E_b = E_{max} - E_{min} \tag{1}$$

where E_{max} and E_{min} are the maximum and minimum supercell image energies, respectively, along the migration pathway.

Material descriptor formulation, formulation of DFT-E_b-based search/screening driven by BO.
Candidate material descriptors were extracted from the DFT-optimized crystal structures, their description is available in Supplementary Table S1 and Supplementary Figure 1. The resulting initial domain size of the feature space has a total of 348 descriptors. Details on the construction of additive Bayesian model are provided as well in Supplementary Information section.

References

1. Nishijima, M. *et al*. Accelerated discovery of cathode materials with prolonged cycle life for lithium-ion battery. *Nat. Commun.* **5**, 4553 (2014).
2. Jain, A. *et al*. The Materials Project: A materials genome approach to accelerating materials innovation. *APL Materials* **1**, 011002 (2013).
3. Hautier, G., Fischer, C., Ehrlacher, V., Jain, A. & Ceder, G. Data mined ionic substitutions for the discovery of new compounds. *Inorg. Chem.* **50**, 656–663 (2011).
4. Meredig, B. *et al*. Combinatorial screening for new materials in unconstrained composition space with machine learning. *Phys. Rev. B* **89**, 094104 (2014).
5. Sun, W. *et al*. The thermodynamic scale of inorganic crystalline metastability. *Sci. Adv.* **2**, e1600225 (2016).
6. Hohenberg, P. & Kohn, W. Inhomogeneous electron gas. *Phys. Rev.* **136**, B864–B871 (1964).
7. Kohn, W. & Sham, L. J. Self-consistent equations including exchange and correlation effects. *Phys. Rev.* **140**, A1133–A1138 (1965).
8. Kirklin, S. *et al*. The Open Quantum Materials Database (OQMD): assessing the accuracy of DFT formation energies. *NPJ Comput. Mater.* **1**, 15010 (2015).
9. Ceder, G., Hautier, G., Jain, A. & Ong, S. P. Recharging lithium battery research with first-principles methods. *MRS Bulletin* **36**, 185–191 (2011).
10. Aykol, M. & Wolverton, C. Local environment dependent GGA + U method for accurate thermochemistry of transition metal compounds. *Phys. Rev. B* **90**, 115105 (2014).
11. Liu, M. *et al*. Spinel compounds as multivalent battery cathodes: a systematic evaluation based on *ab initio* calculations. *Energy Environ. Sci.* **8**, 964–974 (2015).
12. Fujimura, K. *et al*. Accelerated materials design of lithium superionic conductors based on first-principles calculations and machine learning algorithms. *Adv. Energy Mater.* **3**, 980–985 (2013).
13. Jalem, R., Kimura, M., Nakayama, M. & Kasuga, T. Informatics-aided density functional theory study on the Li ion transport of Tavorite-type LiMTO₄F (M^{3+}–T^{5+}, M^{2+}–T^{6+}). *J. Chem. Inf. Model.* **55**, 1158–1168 (2015).

14. Genreith-Schriever, A. R., Hebbeker, P., Hinterberg, J., Zacherle, T. & De Souza, R. A. Understanding oxygen-vacancy migration in the Fluorite Oxide CeO_2: An *ab initio* study of impurity-anion migration. *J. Phys. Chem. C* **119**, 28269–28275 (2015).

15. Nakayama, M., Yamada, S., Jalem, R. & Kasuga, T. Density functional studies of olivine-type $LiFePO_4$ and $NaFePO_4$ as positive electrode materials for rechargeable lithium and sodium ion batteries. *Solid State Ionics* **286**, 40–44 (2016).

16. Jalem, R., Natsume, R., Nakayama, M. & Kasuga, T. First-principles investigation of the Na^+ ion transport property in oxyfluorinated Titanium(IV) Phosphate $Na_3Ti_2P_2O_{10}F$. *J. Phys. Chem. C* **120**, 1438–1445 (2016).

17. Jalem, R., Nakayama, M. & Kasuga, T. Alkali ion transport in Tavorite-type $ABTO_4X$ (A: Li, Na; B-T: Al-P, Mg-S; X: F). *Electrochemistry* **82**, 851–854.

18. Adams, S. Bond valence analysis of structure-property relationships in solid electrolytes. *J. Power Sources* **159**, 200–204 (2014).

19. Balachandran, P. V., Broderick, S. R. & Rajan, K. Identifying the 'inorganic gene' for high-temperature piezoelectric perovskites through statistical learning. *Proc. R. Soc. A* **467**, 2271–2290 (2011).

20. Mizushima, K., Jones, P. C., Wiseman, P. J. & Goodenough, J. B. Li_xCoO_2 ($0 < x < -1$): A new cathode material for batteries of high energy density. *Mater. Res. Bull.* **15**, 783–789 (1980).

21. Rougier, A., Gravereau, P. & Delmas, C. Optimization of the composition of the $Li_{1-z}Ni_{1+z}O_2$ electrode materials: Structural, magnetic, and electrochemical studies. *J. Electrochem. Soc.* **143**, 1168–1175 (1996).

22. Padhi, A., Nanjundaswamy, K. & Goodenough, J. B. Phospho-olivines as positive-electrode materials for rechargeable lithium batteries. *J. Electrochem. Soc.* **144**, 1188–1194 (1997).

23. Murugan, R., Thangadurai, V. & Weppner, W. Fast lithium ion conduction in Garnet-type $Li_7La_3Zr_2O_{12}$. *Angew. Chem. Int. Ed.* **46**, 7778–7781 (2007).

24. Kamaya, N. *et al.* A lithium superionic conductor. *Nat. Mater.* **10**, 682–686 (2011).

25. Richards, W. D. *et al.* Design and synthesis of the superionic conductor $Na_{10}SnP_2S_{12}$. *Nat. Commun.* **7**, 11009 (2016).

26. Kiyohara, S., Oda, H., Tsuda, K. & Mizoguchi, T. Acceleration of stable interface structure searching using a kriging approach. *Jpn. J. Appl. Phys.* **55**, 045502 (2016).

27. Bartók, A. P., Payne, M. C., Kondor, R. & Csányi, G. Gaussian approximation potentials: The accuracy of quantum mechanics, without the electrons. *Phys. Rev. Lett.* **104**, 136403 (2010).

28. Toyoura, K. *et al.* Machine-learning-based selective sampling procedure for identifying the low-energy region in a potential energy surface: A case study on proton conduction in oxides. *Phys. Rev. B* **93**, 054112 (2016).

29. Seko, A., Maekawa, T., Tsuda, K. & Tanaka, I. Machine learning with systematic density-functional theory calculations: Application to melting temperatures of single- and binary-component solids. *Phys. Rev. B* **89**, 054303 (2014).

30. Seko, A. *et al.* Prediction of low-thermal-conductivity compounds with first-principles anharmonic lattice-dynamics calculations and bayesian optimization. *Phys. Rev. Lett.* **115**, 205901 (2015).

31. Balachandran, P. V., Xue, D., Theiler, J., Hogden, J. & Lookman, T. Adaptive strategies for materials design using uncertainties. *Sci. Rep.* **6**, 19660 (2016).

32. Li, Y., Han, J. –T., Wang, C.–A., Xie, H. & Goodenough, J. B. Optimizing Li^+ conductivity in a garnet framework. *J. Mater. Chem.* **22**, 15357–15361 (2012).

33. Whittingham, M. S. Lithium Batteries and Cathode Materials. *Chem. Rev.* **104**, 4271–4302 (2004).

34. Yang, S. *et al.* $Na_3[Ti_2P_2O_{10}F]$: A New Oxyfluorinated Titanium Phosphate with an Ionic Conductive Property. *Chem. Mater.* **19**, 942–947 (2007).

35. Ma, Z. *et al.* Experimental visualization of the diffusion pathway of sodium ions in the $Na3[Ti_2P_2O_{10}F]$ anode for sodium-ion battery. *Sci. Rep.* **4**, 7231 (2014).

36. Recham, N. *et al.* A 3.6 V lithium-based fluorosulphate insertion positive electrode for lithium-ion batteries. *Nat. Mater.* **9**, 68–74 (2010).

37. Sebastian, L., Gopalakrishnan, J. & Piffard, Y. Synthesis, crystal structure and lithium ion conductivity of $LiMgFSO_4$. *J. Mater. Chem.* **12**, 374–377 (2002).

38. Rangaswamy, P., Suresh, G. S. & Kittappa, M. M. A new tavorite $LiTiPO_4F$ electrode material for aqueous rechargeable lithium ion battery. *J. Solid State Electrochem.* **20**, 2619–2631 (2016).

39. Wang, Z., Zoghi, M., Hutter, F., Matheson, D. & De Freitas, N. Bayesian optimization in high dimensions via random embeddings. *In Proceedings of the Twenty-Third international joint conference on Artificial Intelligence*, 1778–1784 (2013).

40. Djolonga, J., Krause, A. & Cevher, V. High-dimensional gaussian process bandits. *In Advances in Neural Information Processing Systems*, 1025–1033 (2013).

41. Jones, D. R. A taxonomy of global optimization methods based on response surfaces. *J. Global Optim.* **21**, 345–383 (2001).

42. Kandasamy, K., Schneider, J. G. & Poczos, B. High dimensional bayesian optimisation and bandits via additive models. *In Proceedings of the 32nd International Conference on Machine Learning, ICML 2015*, 295-304 (2015).

43. Momma, K. & Izumi, F. VESTA: a three-dimensional visualization system for electronic and structural analysis. *J. Appl. Crystallogr.* **41**, 653–658 (2008).

44. Shannon, R. D. Revised effective ionic radii and systematic studies of interatomic distances in halides and chalcogenides. *Acta Cryst.* **A32**, 751–767 (1976).

45. Inaguma, Y. *et al.* High ionic conductivity in lithium lanthanum titanate. *Solid State Commun.* **86**, 689–693 (1993).

46. Barber, C. B., Dobkin, D. P. & Huhdanpaa, H. The Quickhull Algorithm for convex hulls. *ACM Trans. Math Software* **22**, 469–483 (1996).

47. Ong, S. P. *et al.* Python Materials Genomics (pymatgen): A robust, open-source python library for materials analysis. *Comput. Mater. Sci.* **68**, 314–319 (2013).

48. Thompson, T. *et al.* Electrochemical window of the Li-ion solid electrolyte $Li_7La_3Zr_2O_{12}$. *ACS Energy Lett.* **2**, 462–468 (2017).

49. Ong, S. P. *et al.* Phase stability, electrochemical stability and ionic conductivity of the $Li_{10\pm1}MP_2X_{12}$ (M = Ge, Si, Sn, Al or P, and X = O, S or Se) family of superionic conductors. *Energy Environ. Sci.* **6**, 148–156 (2013).

50. Recham, N. *et al.* Ionothermal Synthesis of Li-Based Fluorophosphates Electrodes. *Chem. Mater.* **22**, 1142–1148 (2010).

51. ICSD, Inorganic Crystal Structure Database; http://icsd.fizkarlsruhe.de/icsd/ (2006).

52. Oganov, A. R., Lyakhov, A. O. & Valle, M. How evolutionary crystal structure prediction works - and why. *Acc. Chem. Res.* **44**, 227–237 (2011).

53. Ohta, S., Kobayashi, T. & Asaoka, T. High lithium ionic conductivity in the garnet-type oxide $Li_{7-X}La_3(Zr_{2-X},Nb_X)O_{12}$ (X = 0–2). *J. Power Sources* **196**, 3342–3345 (2011).

54. Kresse, G. & Furthmüller, J. Efficient iterative schemes for ab initio total-energy calculations using a plane-wave basis set. *Phys. Rev. B* **54**, 11169–11186 (1996).

55. Kresse, G. & Joubert, D. From ultrasoft pseudopotentials to the projector augmented-wave method. *Phys. Rev. B* **59**, 1758–1775 (1998).

56. Csonka, G. I. *et al.* Assessing the performance of recent density functionals for bulk solids. *Phys. Rev. B* **79**, 155107 (2009).

57. Bader, R. *Atoms in Molecules: A Quantum Theory*, Oxford University Press, New York (1990).

58. Gonze, X. & Lee, C. Dynamical matrices, Born effective charges, dielectric permittivity tensors, and interatomic force constants from density-functional perturbation theory. *Phys. Rev. B* **55**, 10355–10368 (1997).

59. Jonsson, H., Mills, G., Jacobsen, K. M. in: Berne BJ, Ciccotti G, Coker DF(Eds.), *Classical and Quantum Dynamics in Condensed Phase Simulations*, World Scientific, Singapore (1998).

Acknowledgements

Author Contributions

R.J., M.N., H.Y., and T.S. conceived and directed the work, generated the DFT datasets, and built the material descriptor set. K.K. and I.T. contributed on statistical analyses and on the machine learning aspect of the study. R.J. wrote the manuscript with contributions from M.N., K.K., and I.T.

Additional Information

Supplementary information accompanies this paper at https://doi.org/10.1038/s41598-018-23852-y.

Competing Interests: The authors declare no competing interests.

Publisher's note: Springer Nature remains neutral with regard to jurisdictional claims in published maps and institutional affiliations.